Order Number 1348845

Hypersonic flow over a delta wing at mach 8

Fuller, Douglas Evan, M.S.

The University of Texas at Arlington, 1992

U·M·I

300 N. Zeeb Rd.
Ann Arbor, MI 48106

HYPERSONIC FLOW OVER A DELTA WING AT MACH 8

The members of the Committee approve the masters thesis of Douglas E. Fuller.

Frank K. Lu
Supervising Professor

Donald R. Wilson

David S. Thompson

HYPERSONIC FLOW OVER A DELTA WING AT MACH 8

by

DOUGLAS EVAN FULLER

Presented to the faculty of the Graduate School of
The University of Texas at Arlington in Partial Fulfillment
of the Requirements
for the Degree of

MASTER OF SCIENCE IN AEROSPACE ENGINEERING

THE UNIVERSITY OF TEXAS AT ARLINGTON
May 1992

ACKNOWLEDGMENTS

I would like to express my appreciation to my supervising professor, Dr. Frank K. Lu, for his patience, guidance, and assistance during this experimental program.

I also thank Mr. Jim H. Holland for his technical support during this project. Without his expertise this experiment would not have happened.

Assistance from Mr. Kung-Ming Chung proved invaluable as well as his patience, in completing this experiment.

Special thanks go to my wife, Julie, for her support and encouragement.

April 8, 1992

ABSTRACT

HYPERSONIC FLOW OVER A DELTA WING AT MACH 8

Publication No. _____

Douglas E. Fuller, M.S.

The University of Texas at Arlington

Supervising Professor: Frank K. Lu

A series of experiments was performed at M = 8.0 using a planar delta wing with sharp leading edges swept at 70 degrees. The focus of the experiments was to determine the effects of changing angle-of-attack on the leeward flowfield. Surface oil-flow visualizations were taken to understand the flowfield over the leeside region. Surface pressure data was taken near the trailing edge of the model to show pressure trends and provide more detail of flowfield characteristics. Analysis of the results led to a description of the principal features of the flowfield.

TABLE OF CONTENTS

LIST OF FIGURES

LIST OF TABLES

NOMENCLATURE

AOA = angle of attack

c = chord

M_∞ = freestream Mach number

M_n = Mach number normal to the leading edge

$= M \cos \Lambda \, (1 + \sin^2 \alpha \tan^2 \Lambda)^{1/2}$

Re = Reynolds number

$= U_\infty \, c \, / \, \mu_\infty$

s = semi-span

t/c = thickness/chord ratio

U_∞ = freestream velocity

α = angle of attack

α_n = angle of attack normal to the leading edge,

$= \tan^{-1}(\tan \alpha \sec \Lambda)$

Λ = wing sweep

μ_∞ = dynamic viscosity

τ = outflow angle

CHAPTER 1

INTRODUCTION

Wings of low aspect ratio are of continuing interest in the development supersonic military aircraft and hypersonic vehicles. The exploration of the leeside flowfield at high Mach numbers and over a wide range of angles of attack is necessary for the effective development of the newest fighter aircraft and next generation reentry vehicles. Miller and Wood [5] did extensive research into low Mach number supersonic flow on a variety of sharp leading edge delta wings. They classified the surface flow into seven distinct types, depending on the flow observed. Hillier [3] and Webster and Shang [18] both provided a low Mach number, low angle of attack numerical approach that duplicated some of the results from experimental studies. Published work at freestream Mach numbers greater than four has been sparse and understanding of leeside flowfields is far from complete. Work by Rao [8] and Narayan [6] has expanded the knowledge base into higher Mach numbers. There have also been numerical studies of the leeside flow [10,17]. This project is designed to further broaden our knowledge of leeside flowfield at higher Mach numbers.

1.1 Review of Leeside Flowfields

The leeside flowfield is complex and depends on many variables including wing sweep, thickness, Reynolds number, Mach number, and angle of attack. Previous work by Stanbrook and Squire [12,13,14] and others [2,9,11,18] have concentrated on $M_n < 2.0$, where M_n is the Mach number normal to the leading edge. Three flow regimes can be identified as shown in figure 1 (this figure includes details that will be discussed later). The boundary between the subsonic and supersonic leading edges is commonly referred to as the Stanbrook-Squire boundary. To the left of the boundary the flow is always separated (region A). To the right of the boundary the flow is attached at the leading edge at low and moderate α_n, α_n being the angle of attack normal to the leading edge, although shock-induced separations may occur inboard of the edges. At very high α_n the flow detaches from the leading edge into an unsteady turbulent wake. The boundary between shock detachment and detachment at the leading edge at both low and high α_n is also indicated in figure 1. Below this boundary both separated and attached flow seem to be present, although the uncertainty in determining the type of flow within this region may be due to the difficulty in observing the flow at the leading edge [1,13]. The present experiments concentrate on the regime to

the far right of the Stanbrook-Squire boundary (figure 1), examining the effects of angle of attack changes.

The primary features of the hypersonic flowfield are shown in perspective in figure 2. The windward side has a conical shock that is attached at the leading edge. At very high α_n, however, the windward shock is detached, causing flow leakage past the detached edges. The leeside flow is also typically turbulent and unsteady. Earlier work by Cross and Hankey [1] has broken down the two regimes to the right of the Stanbrook-Squire boundary in figure 1 (B & C) into three distinct flowfield regimes. This was later refined by Narayan [6] who classified this region into four flowfield regimes (figure 3) with the following characteristics: 1) attached, quasi-parallel flow at very low α_n without vortices below the shock-attachment line; 2) attached, quasi-parallel flow with embedded vortices; 3) shock induced separation along inboard rays; and 4) leading edge separation at high α_n (figure 3). These regimes were defined at a freestream Mach number of 10. At very small α_n the bow shock is attached and a viscous layer with attached, quasi-parallel flow is present. A weak realignment shock exists on both sides of center (figure 3a). This realignment shock is embedded in the inviscid flow, as an oblique shock, to realign the incoming inviscid flow to parallel the plane of symmetry. As the angle of attack increases the realignment shock gains in strength until it causes the flow to first show embedded vortices (figure 3b)

and then a shock-induced separation of the viscous flow (figure 3c). The vortices increase in size as the realignment shock strength increases. Finally, as α_n increases to the point where the leading edge shock separates, multiple vortices and shocks occur in the turbulent wake (figure 3d).

1.2 Trailing Edge Effects

The trailing edge of the delta wing normally does not play an important role in the flow on the leeside of a delta wing. At high angle of attack this no longer holds true. Evidence of flow around the trailing edge against the leeside flow at high angle of attack was mentioned by Squire [12], Cross and Hankey [1], and Webster and Shang [18]. At a high angle of attack, a recompression shock forms at the rear of the wing. This recompression shock is caused by the overexpansion of the flow around the front part of the wing. As α increases, this shock migrates up the wing. Behind this shock is an area of high pressure turbulent flow. Air flows around the trailing edge from the high pressure windward side and expands onto the relatively low pressure trailing edge region on the leeward side, causing a weak flow reversal on the leeward side.

1.3 Reynolds Number Effects

Szodruch [15] found the Reynolds number affects not only the shape of the separation bubble and pressure level near the leading edge but the type of flow around the wing as well. He found that Reynolds number only affects the vortex center position, vortex size, and pressure level near the leading edge. Vortex intensities increase with increasing Re, and this increase in vortex intensity becomes very pronounced as Re increases past 4 x 10 . At higher angles of attack, the flow becomes turbulent and a pair of strong primary vortices dominate the flowfield, with no noticeable Re effects in the experiments. Further work on Reynolds number effects can be found in Szodruch and Peake [16] and Whitehead [19].

CHAPTER 2

EXPERIMENTAL PROGRAM

2.1 Facility

The experiments were performed in the University of Texas at Arlington's Hypersonic Shock Tunnel Facility (figure 4). The shock tunnel operated in the reflected mode and was of conventional design. The tunnel was separated into three independently pressurized parts by diaphragms. A high-pressure driver tube, 6 in. (150 mm) in diameter and 10 ft (3 m) long was connected, through a double-diaphragm section, to a 6 in. (150 mm) diameter and 27 ft (8.2 m) long driven tube. A secondary diaphragm was used to separate the driven tube gas from that in the test section. The driver tube could be charged to maximum of 6,000 psi (41 MPa). The driven tube has a pressure range from below 0.1 psia (0.7 kPa) to 150 psia (1.0 MPa). The test section could be evacuated to below 0.2 psia (140 Pa). Precise control of the driven and driver tube pressures was achieved by using the double-diaphragm arrangement. This setup produced highly repeatable stagnation conditions and unit Reynolds numbers. At the end of the driven tube was the secondary diaphragm that separated

the driven tube from the test section. Different nozzle throats could be attached prior to the test section, which enable testing at Mach numbers from 5 to 16. The test gas in the driven tube was expanded by a conical nozzle, 101 in.(2.6 m) long, with a 7.5 degree half-angle expansion and an exit diameter of 13.25 in (336 mm). The nozzle was connected to a semi-free jet test section 21.1 in (536 mm) long and 17.5 in (440 mm) in diameter followed by a diffuser and a 150 ft^3 (4.25 m^3) upright, cylindrical dump tank. Test section surveys revealed that the inviscid core was about 6 in (150 mm) in diameter. Test conditions for both the flow visualization and surface pressure measurements were steady at M = 8 and Re = 1.4 x 10 . Estimated run times were in the 4 to 6 ms range.

2.2 Data Acquisition System

Two LeCroy four-channel digitizers with programmable amplifiers were used to acquire the pressure data at a sampling rate of one million samples per second per channel. These digitizers were mounted in a LeCroy CAMAC mainframe. Data were transmitted from the data acquisition system to an Everex Step 286 microcomputer via a LeCroy Interface and a pair of National Instruments bus extenders. The latter were required because the data acquisition mainframe was located over 100 ft (30 m) from the host computer. Eight external

instrumentation amplifier-filters with 100 kHz bandwidth were available for anti-aliasing and also for exploiting the 12-bit digitizing capability of the data acquisition modules.

Surface pressure measurements were made with both flush and internally mounted, miniature high-frequency transducers. The internally mounted transducers were connected to the surface via a 0.1 in. (2.5 mm) diameter stainless steel tube. The transducers and tubing were secured in place using silicone rubber sealant. Kulite Models XCS-093-5A and XCS-093-50A with 0-5 psia (0-35 kPa) and 0-50 psia (0-350 kPa) ranges were used. These transducers had Type "M" protective screens and sensing surfaces of 0.038 in. (0.97 mm) diameter.

Kulite transducers were calibrated against an MKS Baratron Model 127A vacuum gage, a capacitance manometer accurate to ± 0.001 psia (±7 Pa), before the start of each day of runs. A first-order calibration was used. Due to limits on the size of the model imposed by the inviscid test core and the scarcity of pressure transducers only seven transducers were installed on the model.

2.3 Test Model

The delta wing was designed to be as large as possible and still fit inside the estimated 6 in. (150 mm) inviscid core of the wind tunnel at all angles of attack. Figure 5 shows the design of the wing. The aluminum wing had a sweep

of 70° and a leading edge bevel of 10°. both to an accuracy of 0.1°. The base of the wing was 4 in. (102 mm) wide, and the thickness is 0.5 in.(13 mm). This gave a t/c of 0.091. The wing could be pitched to a maximum of 72° measured by a machinist protractor accurate to 0.1°. The wing had a hollowed out chamber at the rear for installing pressure transducers and the associated wiring.

The wing was attached to the tunnel through a clamp-sting setup. Six aluminum clamps were made to hold the delta wing at 0°, 10°, 20°, 30°, 40°, and 50° angle of attack. The delta wing was connected to the clamp with two countersunk screws on the windward side of the delta wing. The clamp was connected to the sting with set screws (Figure 6). The clamp geometry was such that it caused minimum interference to the flow over the wing even at high angles of attack.

2.4 Experimental Techniques

The experiments were done in two parts. The first part was a series of surface flow visualization tests using well-developed techniques [4]. The experiments concluded with a series of surface pressure measurements on the trailing edge of the delta wing.

2.4.1 Surface Flowfield Visualization

A mixture of ground chalk and silicone oil was spotted on the lee surface of the wing. During the test the mixture flowed along lines of surface stress. The trace was then carefully preserved by laying an acetate sheet on the test surface, lifting the sheet, and pressing the sheet onto a piece of paper. This allowed a full-sized image to be obtained for subsequent data analysis.

2.4.2 Pressure Measurements

After the completion of the surface flow visualization tests, a series of runs was made to measure the pressure near the trailing edge. The spanwise surface pressures near the trailing edge assisted in interpreting the surface flow visualizations. The pressure transducers were mounted 0.25 in. (6.35 mm) from the trailing edge (figure 5) to measure a spanwise pressure distribution that covered 75% of the delta wing's span. The pressure taps were spaced 0.25 in. (6.35 mm) apart. By alternating the pressure taps across the wing span, a detailed plot of the wing semi-span pressure can be made due to the symmetry of the flow. This effectively made the pressure measurements 12.5% of the wing semi-span apart. Surface pressure measurements could not be performed near the leading edge of the model due to the sharp leading edge

bevel. The wing was too thin near the leading edge to mount pressure taps.

CHAPTER 3

RESULTS AND DISCUSSION

3.1 Visualization Tests

The results from the visualization tests were consistent with previous research. The present results at low angles of attack were very similar to results obtained at Mach 10 by Narayan [6]. Since very little research has been accomplished at high α_n, the present results at high α_n proved very interesting in showing the formation and growth of a spanwise recompression shock that migrated from the trailing edge to the leading edge as α_n increased. Behind this shock was a relatively low pressure, turbulent region. The flow patterns were also symmetric. The flow visualizations showed a weak reverse flow up the delta wing from the windward side, as previously observed by both Squire [13] and Narayan [6] (figures 7a - 7f).

The surface flow over the delta wing fell into three of the four regions explored by Narayan [6] (figure 3). At α = 0° the surface flow over the delta wing was attached and formed parallel lines the length of the wing. The visualizations indicated that at the leading edge a small vortex

had formed with the reattachment line very near the leading edge (figure 7a). At $\alpha = 10°$, the surface flow visualizations indicated that the flow still was attached at the leading edges, but the presence of vortices was clearer (figure 7b). This corresponded to figure 3b. Separation of the flow occured just inboard of the leading edges. The vortical flowfield, inside the viscous flow, was dominated by vortices that deflected the flow to a outflow angle of 45°. The reattachment line was seen to be close to the centerline. The $\alpha = 20°$ surface flow visualization also indicated that the flow was still attached at the leading edges with a separation line forming jusy invoard of the leading edges (figure 7b). The reattachment line is even closer to centerline than at the 10° case. The outflow angle had increased to 67°. The separation seen in both the 10° and 20° is caused by an unfavorable pressure gradient in the viscous layer, which is the result of the wake recompression shock interacting with the thick boundary layer at the trailing edge of the wing [1]. This becomes more significant as angle-of-attack is increased, slowly compressing the vortices and causing the surface flow to turnd slowly toward the leading edge as the AOA increased. No indications of shock induced separation (figure 3c) were seen in any of the flow visualizations. At $\alpha = 30°$, the surface flow was deflected to 90° from the incoming direction (figure 7d). As shown in table 1, as the AOA increased the outflow angle, the

surface streak deflection as the flow reached the leading edge, increased in a linear manner until perpendicular to the incoming freestream flow. The separation line and reattachment line were straight throughout the length of the delta wing. Unlike Rao [8], no secondary separation was seen inboard of the separation line in the present results. At the three lower AOAs there was no sign of a wake recompression shock on the leeside flowfield.

A recompression shock formed at the base of the delta wing caused by the over-expansion of the flow around the front corner of the body as discussed earlier in Chapter 1. The growth of wake recompression shock and its effects on the lee surface were very pronounced at the higher AOAs. At α = 30°, the recompression shock had attached itself to the lee surface (figure 7d). In front of this shock the surface flow appeared similar to the flow at 20°. The surface flow was still deflected perpendicular to the incoming freestream flow. This deflection could be attributed to the vortex flowfield. The surface streaks deflections were disrupted by the presence of the recompression shock that was roughly triangular in shape. The recompression shock started at the center of the trailing edge and expanded both spanwise and chordwise. At 30° AOA (figure 7d), the area behind the recompression shock extended forward to 32% of the chord length, measured from the base, and 25% of the wing semi-span near where the pressure transducers were mounted. The trans-

ducers were mounted 4.4% of the wing chord from the base. At α = 40°, the recompression shock extended to 48% of the wing chord and covered the entire span of the wing (figure 7e). The recompression shock continued to move forward and outboard on the wing as the AOA was in-creased to at α = 50°, the shock had moved to 81% of the wings chord and covered the entire span of the wing (figure 7f). Flow at the tip still showed the same characteristics as the lower α flows. Behind the recompression shock the flow was thought to be separated into a turbulent wake. At both α = 40° and 50° there were indi-cations of a weak reversed flow at the trailing edge from the surface streak deflections. This confirmed past studies [1,12,18] which also found indications of reversed flow around the trailing edge.

3.2 Pressure Tests

The pressure distribution across the trailing edge of the delta wing at the three low AOAs (0°, 10° & 20°) were similar to previous results of Narayan [6], Nikol'skiy [7], Rao [8], and Richards [9] in that the average spanwise pressure dropped with increasing α. At α = 0°, the pressure was fairly uniform over the trailing edge (figure 8). This corresponded well with the uniform surface flow seen over the trailing edge of the wing in the flow visualization (figure 7a). At α = 10°, the spanwise pressure distribution showed

over a 50% reduction from the $\alpha = 0°$ distribution (figure 8). There was also a definitive rise in the spanwise pressure distribution from the center of the wing proceeding outboard. This pressure rise leveled off at roughly 25% of the wing semi-span and remained constant toward the furthest measured point. This corresponded to the pressure rise outboard of the separation line described by Narayan [6]. The $\alpha = 20°$ pressure and flow visualization results were very similar to the 10° results (figures 8 & 7b respectively). Both the $\alpha = 10°$ and 20° runs were in the second regime described by Narayan [6]. At 20° the semi-span pressure distribution dropped further to average less than 20% of the $\alpha = 0°$ distribution. Also a rise in the spanwise distribution occurred, but at a greater rate of increase and with no leveling of pressure observed. The pressure increased to three times the centerline pressure at 75% of the wing semi-span which was very close to the outboard pressure at $\alpha = 10°$. The entire trailing edge is covered by the vortex flow (figures 7e & 7f) causing the drop in the spanwise pressure distribution from the center to the outboard edges seen in this case.

The spanwise pressure distributions for the three higher α's showed unexpected characteristics. While the lower α's showed a decrease in the average pressure distribution as α was increased the three higher α's showed the reverse as the effects of the wake recompression shock dominated the flow-

field in the vicinity of the pressure transducers. At α = 30° the four inboard transducers were behind the recompression shock. The pressure distribution dropped slowly from centerline towards the shock and then was steady outboard of the shock, at roughly the same pressure as at centerline (figure 8). Outboard of the recompression shock the leading-edge vortices still dominated the flowfield as can be seen in the flow visualizations (figures 7d - 7f). The area between the recompression shock and the separated bow shock contracts as the recompression shock moves up the delta wing chord. At both α = 40° and 50° the spanwise pressure distribution increased from the centerline to the leading edge (figure 8). This rate of increase was greater at the 40° case since the recompression shock was closer to the transducers. The average of the pressure distribution also increased with higher angles of attack. This was caused by the increasing influence of the windward side of the delta wing. The increasing angle of attack increased the windward pressure which in turn caused a steady rise in the pressure in the region behind the recompression shock due to flow leakage.

CHAPTER 4

RECOMMENDATIONS FOR FUTURE RESEARCH & CONCLUSIONS

A further investigation between 20° and 50° angle of attack would provide a better understanding of the growth of the recompression shock. Heat transfer and flowfield surveys would be invaluable in further research. A detailed study of centerline pressure as α increases would detail the movement of the recompression shock forward on the wing.

Detailed surface flow visualizations and pressure measurements on the trailing edge have been obtained on the lee surface on a 70-degree sweptback delta wing at Mach eight. The three regimes described by Narayan [6] were observed. As the angle-of-attack increased the average spanwise pressure distribution dropped until the recompression shock started to interact with the flow at $\alpha = 30°$. As the recompression shock migrated up the wing chord the pressure behind the shock steadily increased. Flow visualizations at high angles of attack showed that reversed flow existed behind the recompression shock. This flow was induced by increasing pressure on the windward side.

APPENDIX A

FIGURES

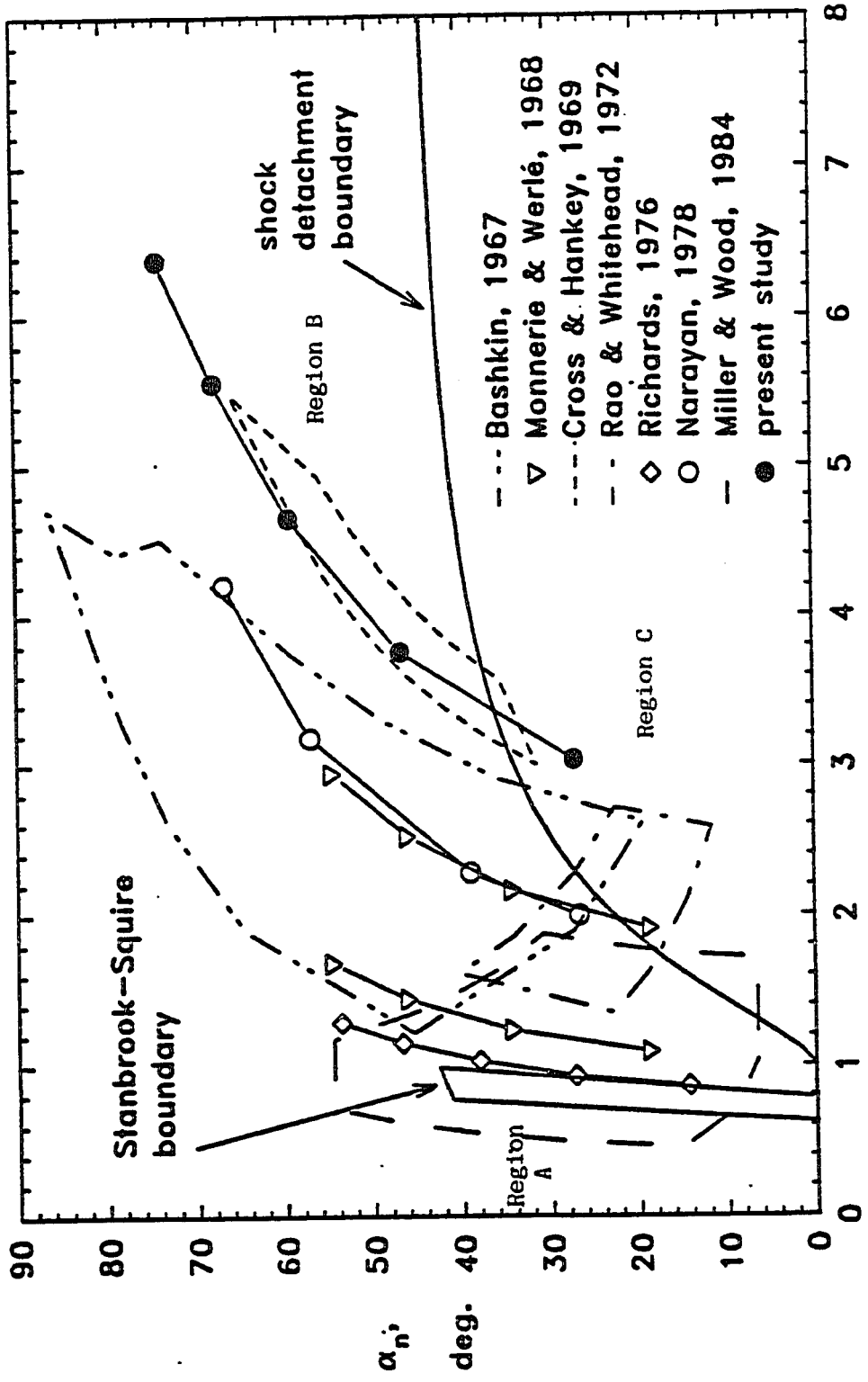

Figure 1: Hypersonic Flow Types

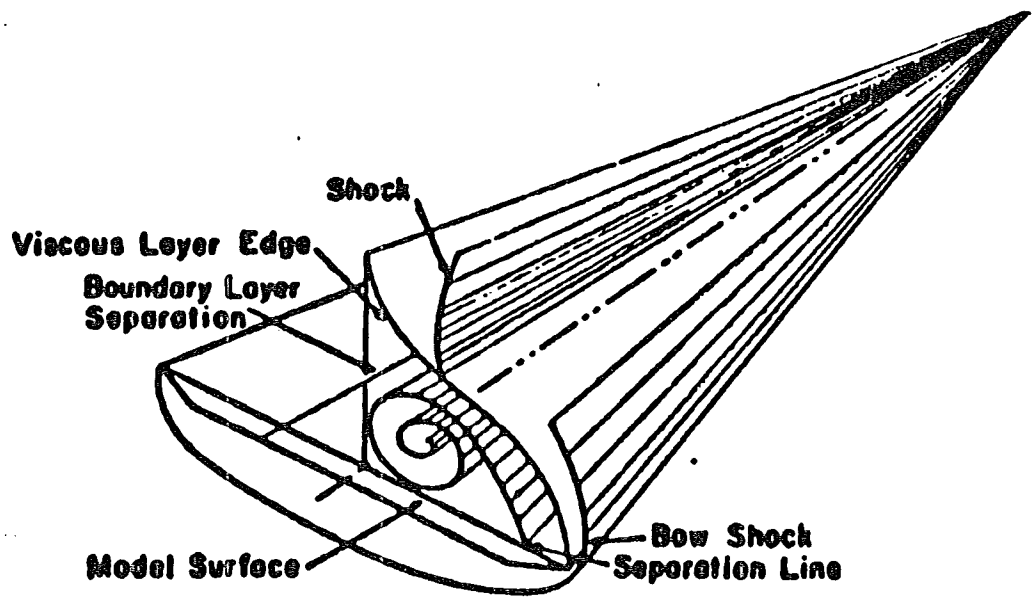

Figure 2: Dominant features of lee-side flowfield
Adapted from Cross and Hankey [1]

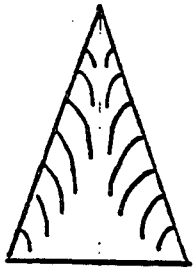

3.a. Attached

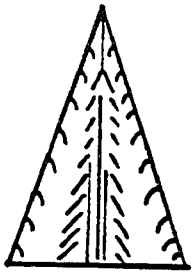

3.b. Attached, with vortices

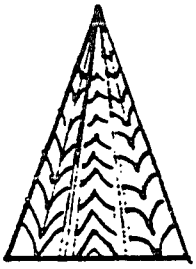

3.c. Shock induced separation

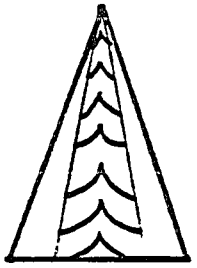

3.d. Leading edge separation

Figure 3: Types of Leeside Flows

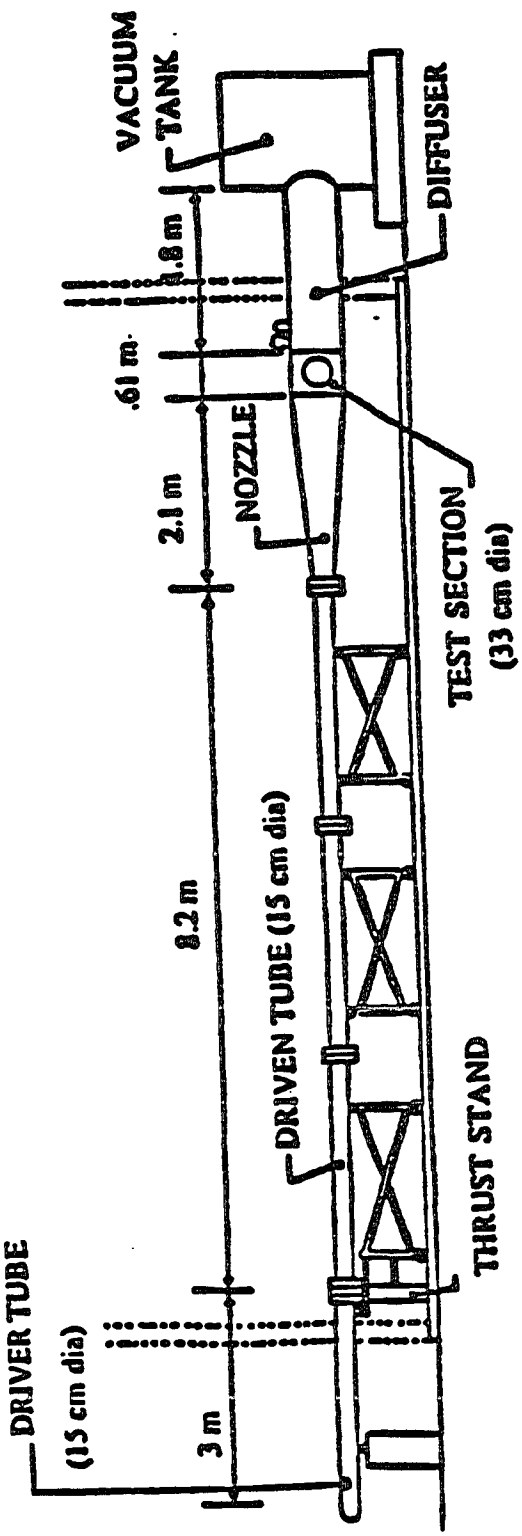

Figure 4: Hypersonic Shock Tunnel

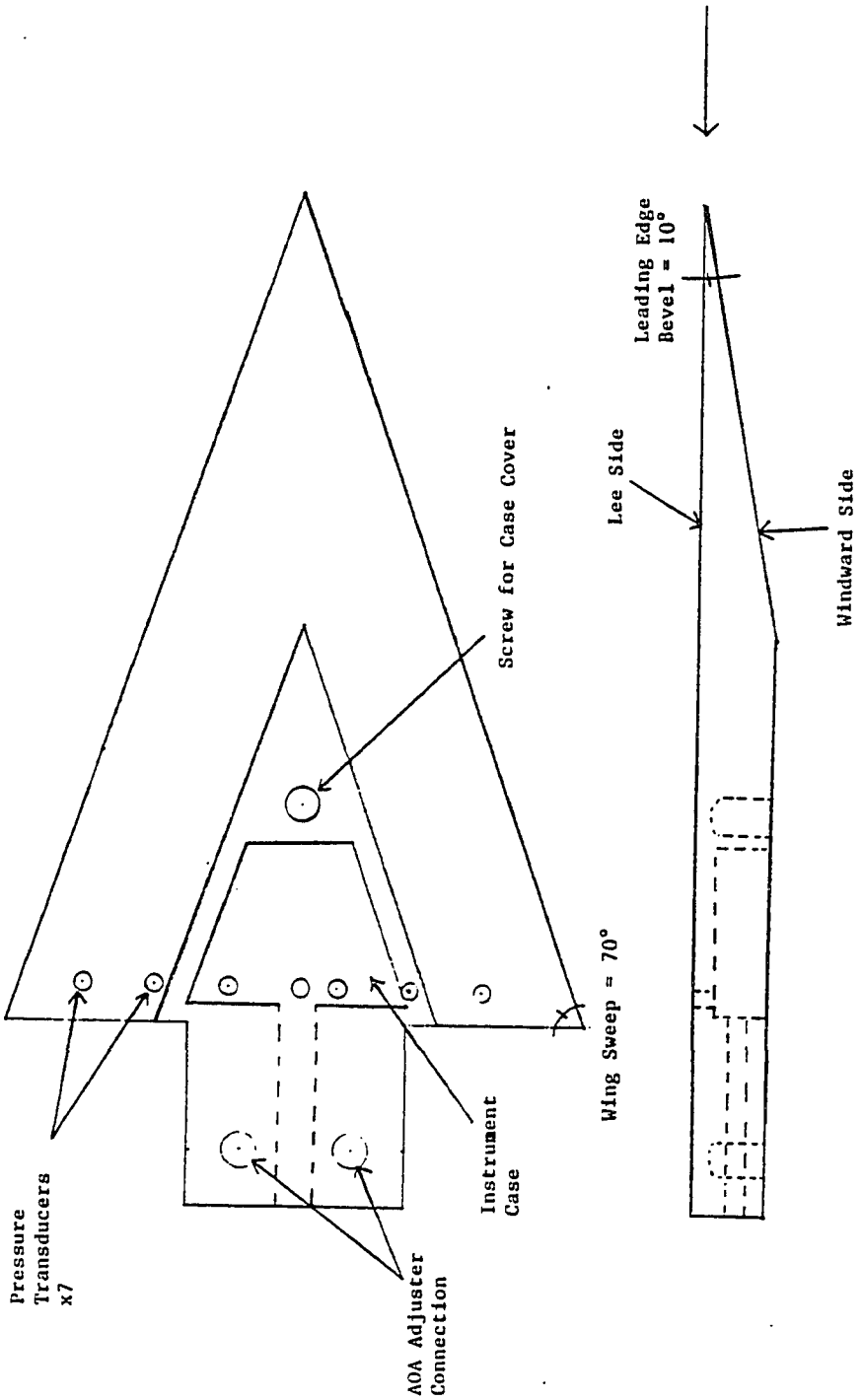

Figure 5: Delta Wing Schematic

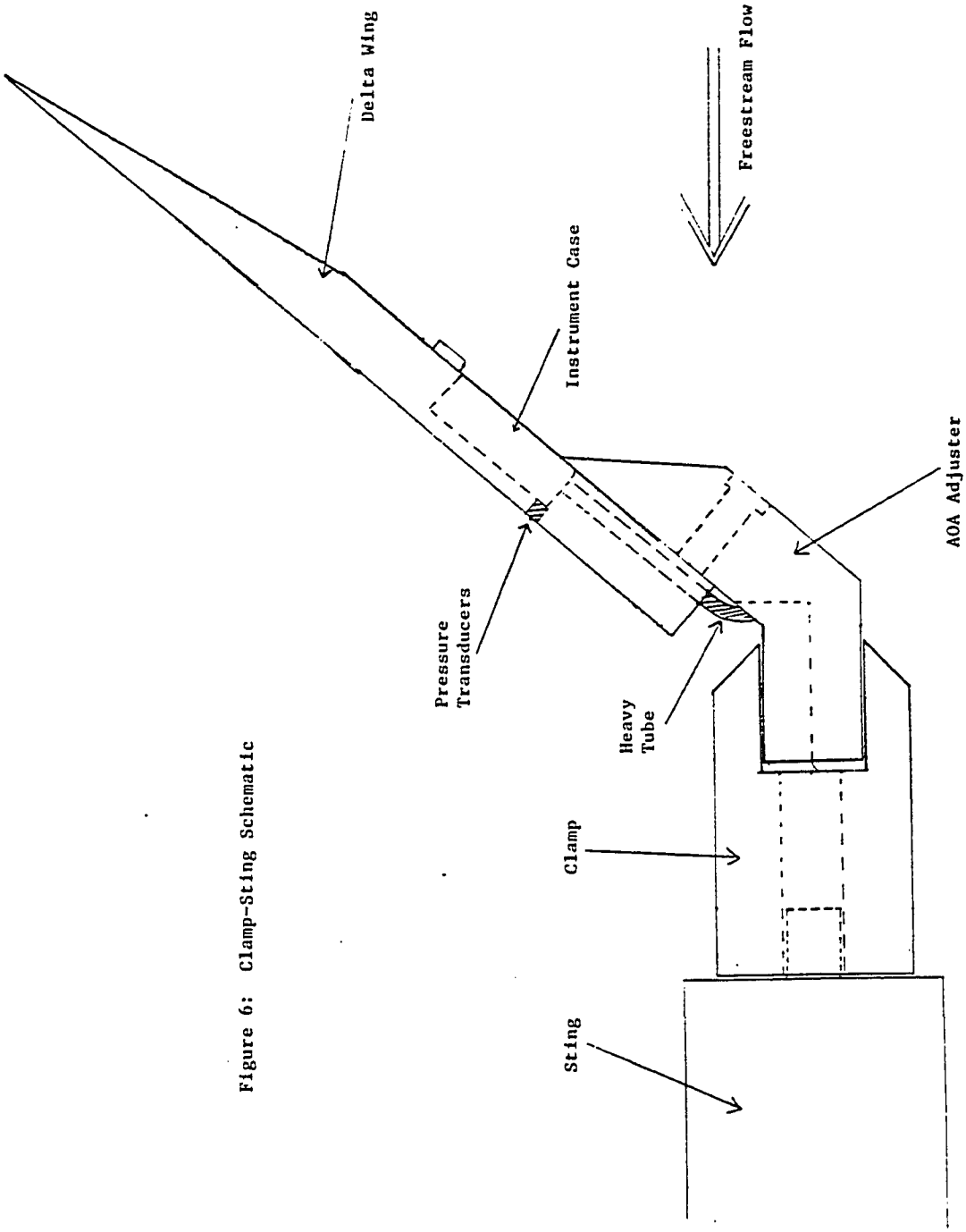

Figure 6: Clamp-Sting Schematic

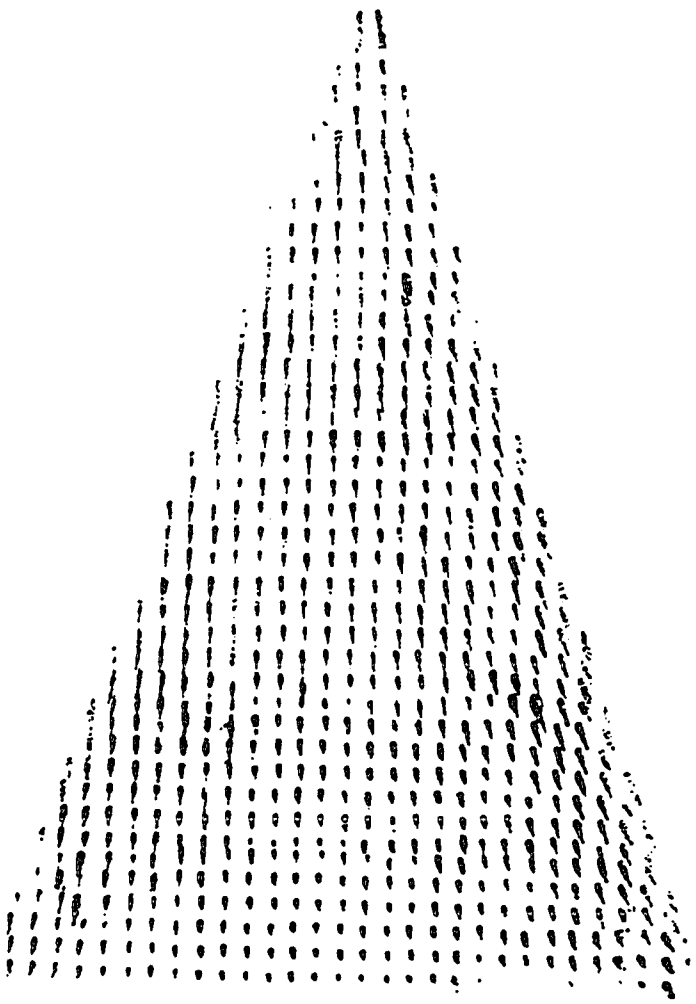

ANGLE OF ATTACK = 0 degrees
Mach = 8.0 Shot # 2

Figure 7.a.

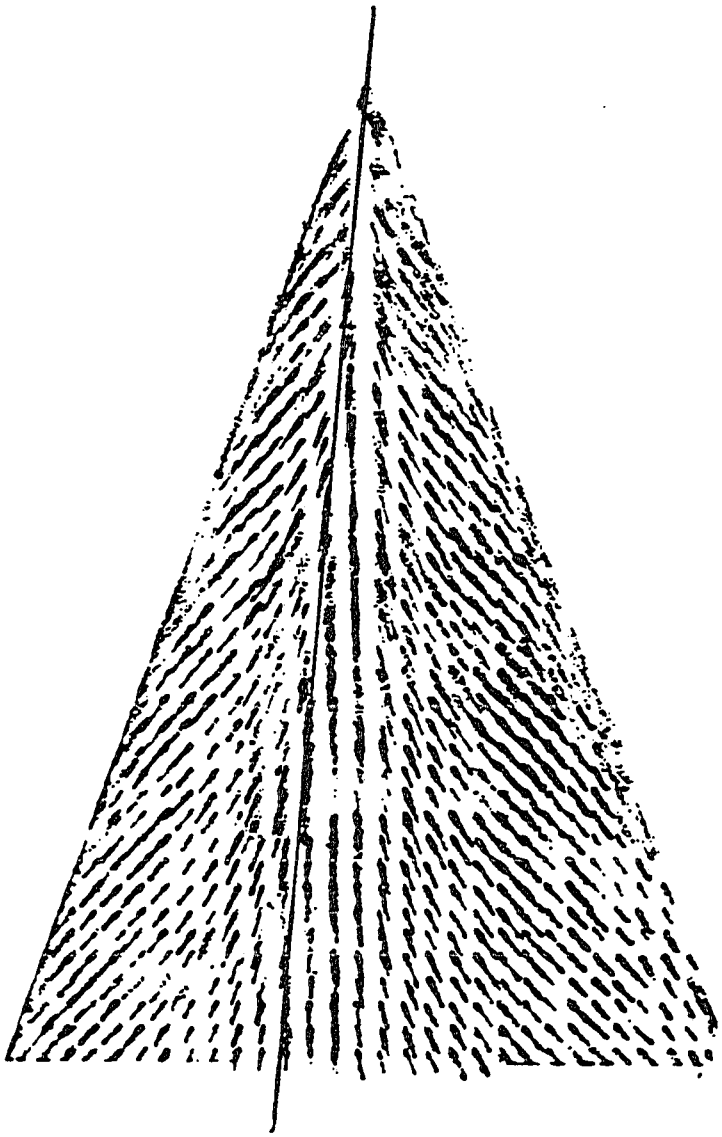

Reattachment Line

ANGLE OF ATTACK = 10 degrees
Mach = 8.0 Shot # 2

Figure 7.b.

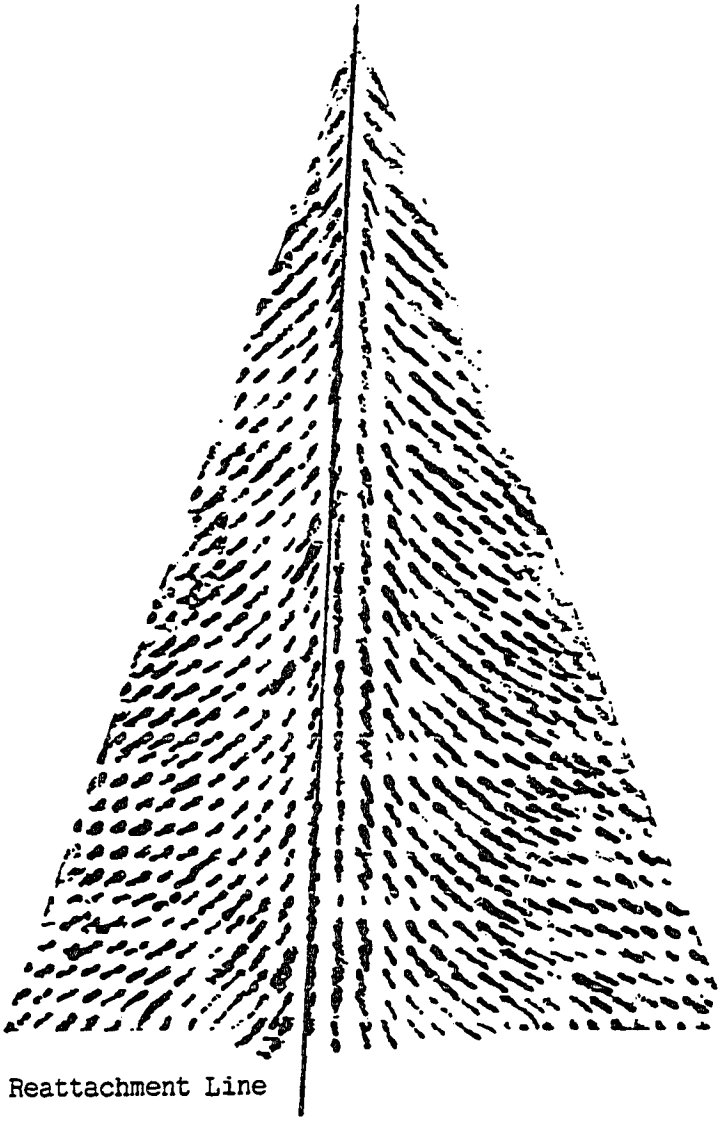

ANGLE OF ATTACK = 20 degrees
Mach = 8.0 Shot # 1

Figure 7.c.

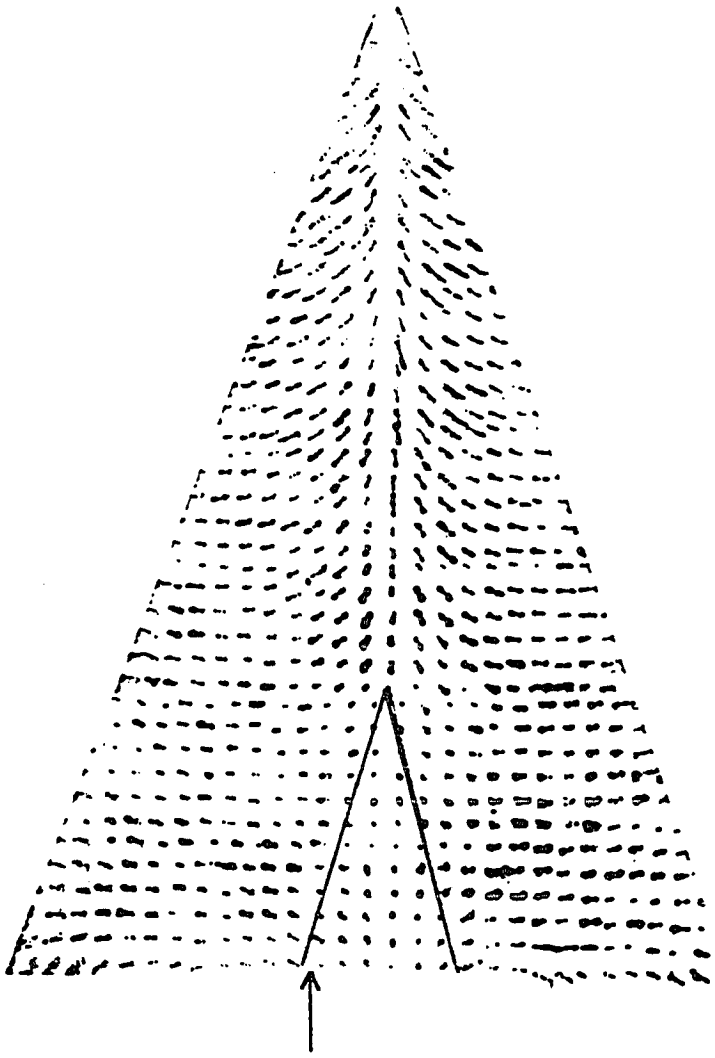

ANGLE OF ATTACK = 30 degrees
Mach = 8.0 Shot # 1

Figure 7.d.

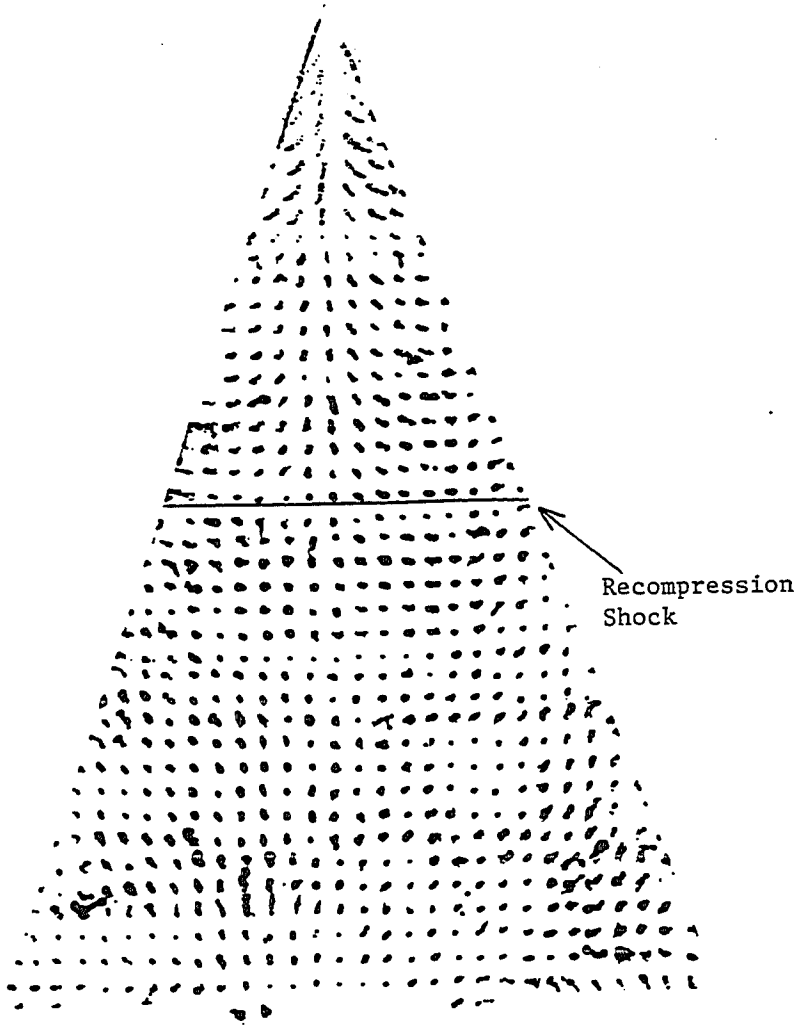

Figure 7.e.
ANGLE OF ATTACK = 40 degrees
Mach = 8.0 Shot # 2

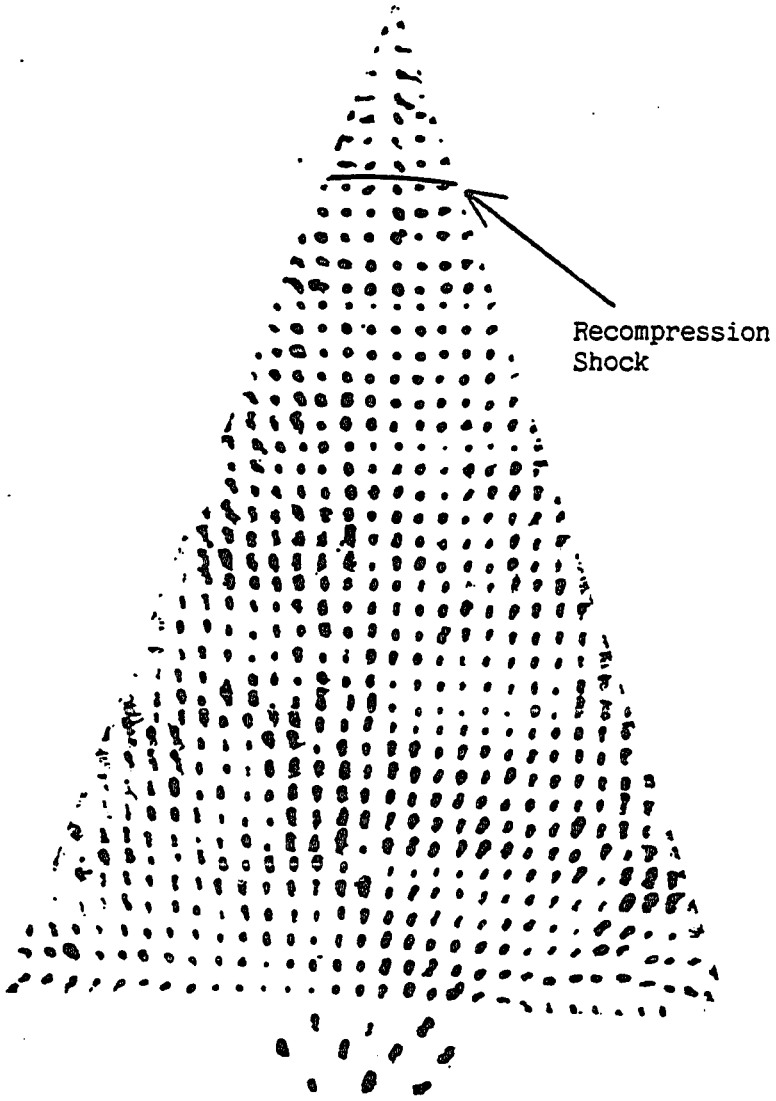

Figure 7.f.
ANGLE OF ATTACK = 50 degrees
Mach = 8.0 Shot # 2

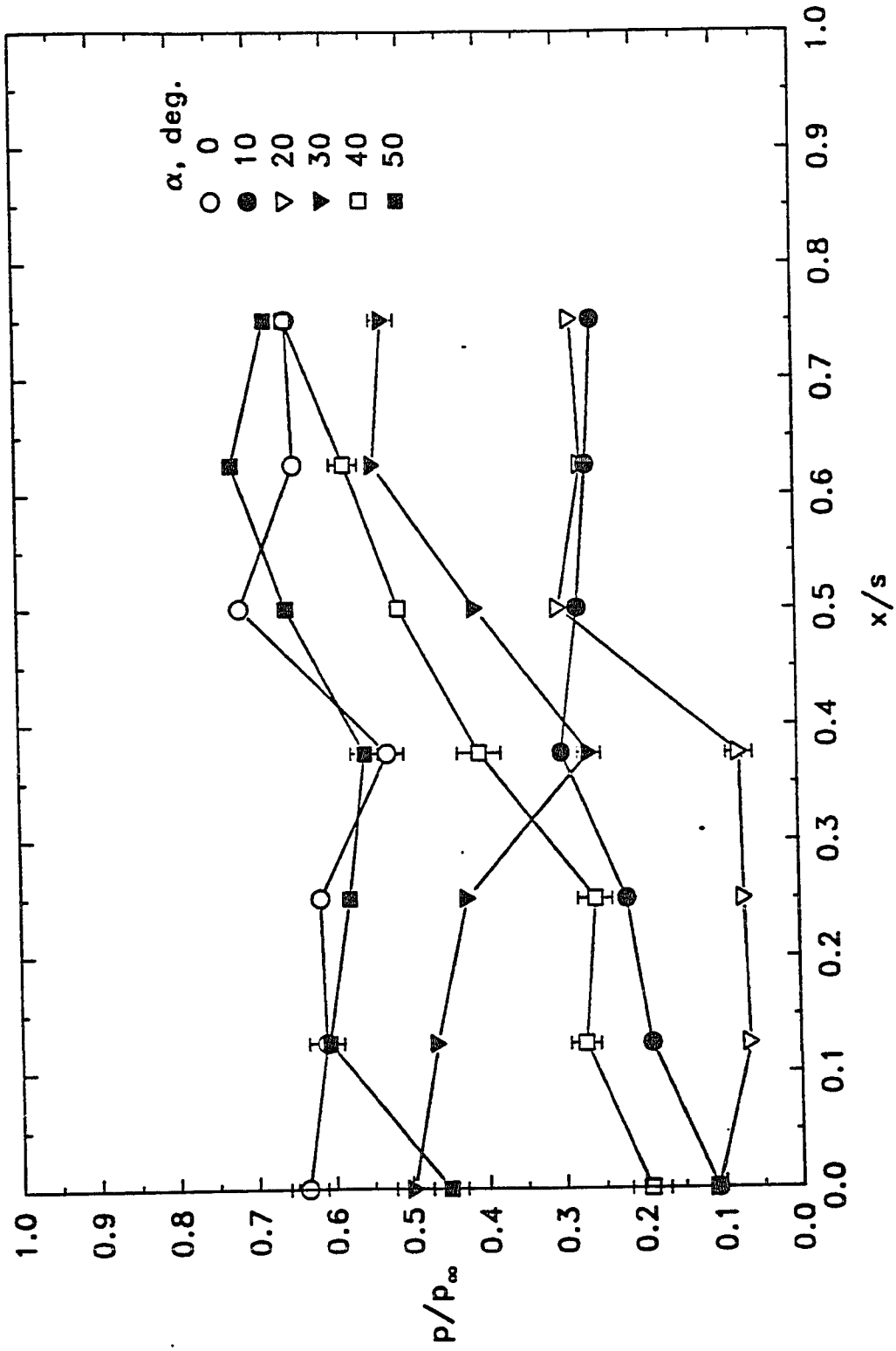

Figure 8: Surface Pressure Measurements

APPENDIX B

TABLES

TABLE 1

OUTFLOW ANGLE

α	α_n	τ
0	0	25
10	27.27	45
20	46.78	67
30	59.36	90
40	67.82	90
50	73.99	90

TABLE 2

BASIC DATA

$M_\infty = 8.0$ $Re = 1.4 \times 10$ $\Lambda = 70°$

Leading edge bevel $[\epsilon] = 20°$ $\epsilon_n = 21.17°$

t/c = 0.091

α	M_n	α_n	α_{neff}	τ	R shock % chord
0°	2.74	0°	21.17°	25°	0
10°	3.03	27.27°	48.44°	45°	0
20°	3.75	46.78°	67.95°	67°	0
30°	4.65	59.36°	80.53°	90°	32
40°	5.55	67.82°	88.99°	90°	55
50°	6.38	73.99°	95.16°	90°	81

REFERENCES

1. Cross, E.J., Jr., and Hankey, W.L., "Investigation of the Leeward Side of a Delta Wing at Hypersonic Speeds," J. Spacecraft, Vol. 6, 1969, pp. 185-190.
2. Ghorai, S.C., "Leading-Edge Vortices and Shock-Detachment Flow over Delta Wings," J. of Aircraft, Vol. 6, 1969, pp.228-232.
3. Hillier, R., "Hypersonic Flow Over Conical Wing-Body Combinations," Aeron. Quart., Vol. XXIX, Nov. 1978, pp 285-304.
4. Lu, F.K. and Settles, G.S., "Color Surface-Flow Visualization of Fin-Generated Shock-wave Boundary-Layer Interactions," Exp. Fluids, Vol. 8, 1989, pp. 352-354.
5. Miller, D.S. and Wood, R.M., "Lee-Side Flow Over Delta Wings at Supersonic Speeds," NASA TP-2430, 1985.
6. Narayan, K.Y., "Leeside Flowfield and Heat Transfer of a Delta Wing at M = 10," AIAA J., Vol 16, 1978, pp. 160-165.
7. Nikol'skiy, Yu.V., "Experimental Study of the Flowfield on the Leeside of a Plate in Viscous Hypersonic Flow," Fluid Mechanics, Soviet Research, Vol. 8, 1979, pp. 39-46.

8. Rao, D.M., "An Experimental Study of the Hypersonic Aerodynamics of Delta Wings," J. Aeron. Soc. India, Vol. 23, 1971, pp. 183-190.

9. Richards, I.C., "Supersonic Flow Past a Slender Delta Wing," Aeron. Quart., May 1976, pp. 143-153.

10. Ruffin S.M. and Murman E.M., "Solutions for Hypersonic Viscous Flow Over Delta Wings," AIAA Paper 88-0126, 1988.

11. Siclari, M.J., "Investigation of Crossflow Shocks on Delta Wings in Supersonic Flow," AIAA J., Vol. 18, 1980, pp. 85-93.

12. Squire, L.C., "Flow Regimes over Delta Wings at Supersonic and Hypersonic Speeds," Aeron. Quart., 1976, pp. 2-14.

13. Squire, L.C., "Leading-Edge Separations and Cross-Flow Shocks on Delta Wings," AIAA J., Vol. 23, 1985, pp. 321-325.

14. Stanbrook, A. and Squire, L.C., "Possible Types of Flow at Swept Leading Edges", Aeron. Quart., Vol. 14, 1964, pp. 72-82.

15. Szodruch, J.G., "Reynolds Number Influence on Lee Side Flow Fields," AIAA J., Vol. 16, 1978, pp. 1306-1309.

16. Szodruch, J.G., and Peake, D.J., "Leeward Flow Over Delta Wings at Supersonic Speeds," NASA TM-81187, 1980.

17. Wardlaw, A.B. Jr. and Davis, S.F., "Euler Solutions for Delta Wings," AIAA J., Vol. 28, 1990, pp. 1826-1829.

18. Webster, W.R. and Shang, J.S., "Numerical Simulation of Reversed Flow over a Supersonic Delta Wing at High Angle of Attack," AIAA Paper 89-1802, 1989.

19. Whitehead, A. H. Jr., Hefner, J. N., and Rao, D.M. "Lee-Surface Vortex Effects Over Configurations in Hypersonic Flow," AIAA Paper 72-77, 1972.